

Article

# The Influence of Process Parameters on the Structure, Phase Composition, and Texture of Micro-Plasma Sprayed Hydroxyapatite Coatings

Xiaomei Liu <sup>1,\*</sup>, Dingyong He <sup>1,2,\*</sup>, Zheng Zhou <sup>1,2</sup>, Zengjie Wang <sup>2</sup> and Guohong Wang <sup>2</sup>

<sup>1</sup> College of Materials Science and Engineering, Beijing University of Technology, Beijing 100124, China; zhouzhengbjut@bjut.edu.cn

<sup>2</sup> Beijing Engineering Research Center of Eco-Materials and LCA, Beijing University of Technology, Beijing 100124, China; wangzj@bjut.edu.cn (Z.W.); wanggh@bjut.edu.cn (G.W.)

\* Correspondence: liuxiaomei@emails.bjut.edu.cn (X.L.); dyhe@bjut.edu.cn (D.H.); Tel.: +86-10-6739-6188 (X.L.)

Received: 8 February 2018; Accepted: 12 March 2018; Published: 15 March 2018

**Abstract:** In this study, hydroxyapatite (HA) coatings were deposited on Ti-6Al-4V by micro-plasma spraying (MPS). The influence of the process parameters on the microstructure of HA coatings was investigated. The splat morphology and spreading behavior were examined to understand the influence of process parameters on the coating. The texture strength of HA coatings was characterized by X-ray diffraction (XRD). The texture coefficients were all applied to characterize the variation in texture. The morphology of splats and coatings were characterized by scanning electron microscopy (SEM). XRD pattern shows that the texture intensity of the *c*-axis of HA was greatly influenced by spraying distance and spraying current. SEM reveals the different texture strength of HA coatings with different ratios of columnar grains. The strongest *c*-axis texture was found in the coating by 60 mm spraying distance with a spraying current of 40 A. In the cross-section SEM images of the coating with the strongest *c*-axis texture, uniform distribution columnar grains were observed in the upper part (~100 μm). The investigation of splats indicates that columnar grain growth occurs after fully melted particles impact the heated substrate. By controlling the melting state prior to in-flight particle impacts, columnar grain growth can be achieved during slow solidification of the disk shape splat during MPS.

**Keywords:** hydroxyapatite; micro-plasma spraying; texture; splat

## 1. Introduction

Hydroxyapatite (HA) coatings have been used as surface coatings on metallic implants because they have a chemical composition similar to that of teeth and bone [1,2], and can stimulate bone growth at the bone implant interface [3]. However, HA has poor bending strength and fracture toughness. It is unsuitable for use in load bearing applications. However, with the rapid development of surface technology, HA coatings deposited by using surface technology on a metal substrate provide excellent biocompatibility and good mechanical properties. The plasma spraying technique is a common method for depositing HA coating on metal implants [4–6]. However, the overheating of HA particles in the plasma jet can cause the decomposition of the HA powders. This leads to the decomposition of HA into tricalcium phosphate (TCP) or tetracalcium phosphate (TTCP) or even toxic calcium oxide (CaO) [7,8]. The rapid cooling rate of the particles on the substrate results in the formation of amorphous calcium phosphate (ACP) [9]. These phases exhibit a fast dissolution rate in the body fluid [10]. The fast dissolution rate of these phases can accelerate implant failure. In order to achieve long-term service, HA coatings with high crystallinity and phase purity is pursued.

Recently, micro-plasma spraying (MPS) has been used to produce HA coatings. MPS, due to its special characteristics, is a feasible thermal spray process for depositing HA coatings on small-scale medical implants [11]. As we know, the phase composition and the microstructure of HA coatings are important factors that influence the properties of these coatings [12]. In turn, these microstructure features depend on the MPS process parameters such as spraying current, plasma gas flow rate, and spraying distance. There have been several reports about the effect of the MPS parameters on the structure and properties of HA coatings [13]. For example, increased spraying power and spraying distance lead to an increase in the crystallinity and phase purity of such coatings. Previous studies also showed that MPS can produce a higher crystallinity (>90%) of HA coatings [14,15].

Many factors influencing the biological and mechanical properties of HA coatings, such as phase composition, crystallinity, surface topography, and grain size [12,16]. Another essential microstructure feature responsible for cell adhesion behavior and the mechanical properties of HA is the crystallographic texture. Several studies on the behavior of a protein adsorbed on different HA crystal surfaces suggested that calcium phosphate materials with texture surfaces may enable control over cellular behavior [17,18]. HA crystals both in long bones and in tooth enamel have preferred orientation in the direction of the *c*-axis. It was reported that hydroxyapatite coatings, compared with randomly oriented coatings, with high *c*-axis orientations have a higher chemical stability [19]. This crystal orientation in HA coatings is promising for long-term and safe applications. In addition, the HA coatings with high *c*-axis orientation have high hardness and Young's modulus values [20]. Therefore, the preparation of HA coatings with *c*-axis orientation might be highly reliable in medical applications. There are several techniques such as radio-frequency thermal plasma spraying (TPS) [20–22] and micro-plasma spray (MPS) [9,14,19] that have been reported to prepare HA coatings with strong (002) crystallographic textures. Compared with radio-frequency (RF)-TPS, MPS can be used to obtain HA coatings with (002) crystallographic textures and high HA content. Although a few studies have investigated the microstructure and properties of MPS coatings [15], the effect of different MPS parameters on texture is still not firmly established.

In the present study, the variation in the phase composition and microstructure of HA coatings with different spray parameters were evaluated. The influence of process parameters on the *c*-axis texture of the coatings was studied. Moreover, through calculation of the texture coefficient, the preferred orientation of crystallites in HA coatings was evaluated. Furthermore, in order to understand the influence of spray parameters on coatings, the splat morphology and spreading behavior were analyzed. This study has important scientific significance and practical value since the coming results will provide a theoretical basis for the controlled preparation of HA coatings that can satisfy the clinical application requirements by MPS.

## 2. Materials and Methods

HA coatings were deposited by micro-plasma spraying (MPS, WDP-1, Beijing University of Technology, Beijing, China) on Ti-6Al-4V plates with dimensions of  $\Phi 15 \text{ mm} \times 2.5 \text{ mm}$ . They were grit-blasted to roughen and clean the surface before deposition. Hydroxyapatite powder (Medicoat AG, Mägenwil, Switzerland) with particle sizes of 45–63  $\mu\text{m}$  was employed as a raw powder for depositing the coatings. The MPS process parameters are shown in Table 1. To study the effect of spraying distance, the spraying current was kept constant at 40 A for all experiments done at different spraying distances. At different currents, the spraying distance was kept constant at 60 mm. The morphologies of raw powders and coatings were observed by scanning electron microscopy (SEM, SU8020, Hitachi, Tokyo, Japan) with an acceleration voltage of 10 kV. SEM observation of the raw powders shows that the powders exhibit a spherical shape (Figure 1a). The high magnification SEM of powder cross-section analysis indicated a porous structure of the raw powder (Figure 1b). The polished and polished-etched cross sections of the coatings were prepared before observation. All samples were coated with a thin gold film using a gold ion sputtering system to make them electrically conductive prior to SEM observation. The phase composition of raw powder and as-sprayed coatings

was qualitatively determined through X-ray diffraction (XRD, D8 ADVANCE, Bruker AXS GMBH, Bruker, Karlsruhe, Germany). The operating conditions were 40 kV and 30 mA using Cu K $\alpha$  radiation source. The scattering angle ranges ( $2\theta$ ) from 20 to 60° with a step size of 0.02°. The infrared thermometer (Smart sensor AR882A, ARCO electronics Ltd., Hong Kong, China) was utilized to test the substrate temperature.

The texture coefficients of as-sprayed coatings were calculated as follows [23,24]:

$$TC(abcd) = \frac{I(abcd) / I_{ICDD}(abcd)}{\frac{1}{N} \sum_{(hkil)-1} I(hkil) / I_{ICDD}(hkil)}$$

where  $I(abcd)$  is the measured intensity of the  $(abcd)$ -peak,  $I_{ICDD}$  is the standard intensity for HA raw powders in the International Centre for Diffraction Data (ICDD), and  $N$  is the number of XRD peaks considered—in our case, (0002), (2131), (1122), and (0004), so  $N = 4$ .

**Table 1.** Micro-plasma process parameters.

Current	Voltage	Flow Rate of Argon	Spraying Distance
20–50 A	25 V	1.3 L/min	60–110 mm

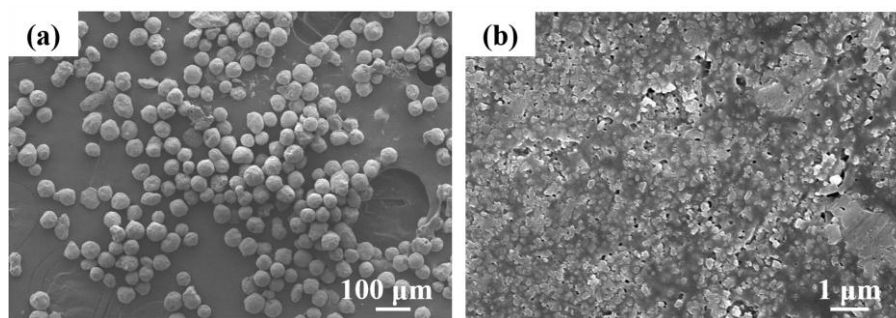


**Figure 1.** Hydroxyapatite (HA) powder morphology: (a) surface morphology; (b) cross-section morphology.

### 3. Results

#### 3.1. Microstructure of As-Sprayed Coatings at Different Spraying Distances

The XRD patterns of as-sprayed HA coatings are shown in Figure 2. The peaks of TTCP and  $\alpha$ -TCP were found in as-sprayed coatings, and the phase CaO could not be identified in the patterns. The peak intensity of TTCP and  $\alpha$ -TCP decreased appreciably when the spraying distance increased from 40 to 60 mm. However, the peaks of TTCP and  $\alpha$ -TCP increased and the amorphous hump became significant when the spraying distance increased from 60 to 110 mm. It should be noted that the XRD patterns of raw powders (Figure 2) show that all diffraction peaks correspond to a standard HA powder pattern (ICDD 09-0432), which indicated that the raw powder exhibits random crystal orientation. However, the intensity of the peaks (0002) and (0004) of as-sprayed coatings increased at short spraying distances (40–80 mm). These results indicate that a preferential orientation of crystals with the (0002) and (0004) planes for the  $c$ -axis texture is formed during MPS deposition.

Figure 3 shows the effect of spraying distance on the preferred  $c$ -axis orientation of the as-sprayed HA coatings. From Figure 3, it is clear that TC (0002) and TC (0004) increased when the spraying distance increased from 40 to 60 mm. This illustrates that the  $c$ -axis texture improved by increasing the spraying distance. However, TC (0002) and TC (0004) decreased significantly when the spraying distance increased from 60 to 110 mm. Thus, the texture intensity greatly decreases in this case. These results indicated that the spraying distance had a significant influence on the texture intensity of HA coatings.

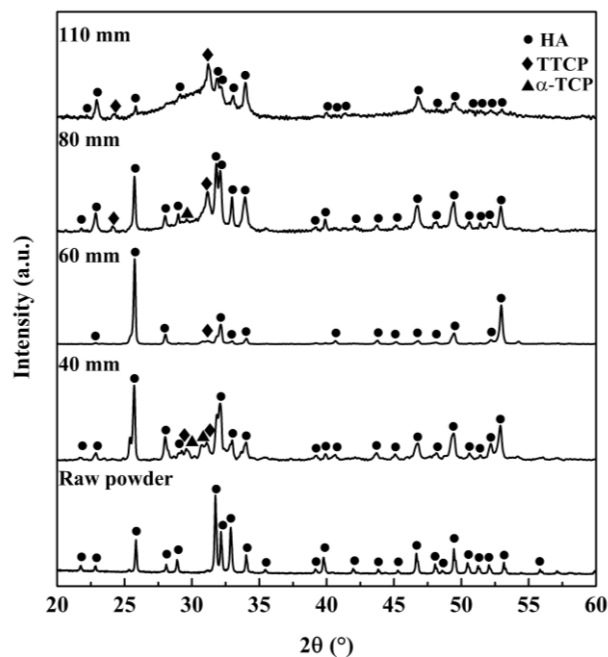


Figure 2. XRD patterns of HA coatings with different spraying distances.

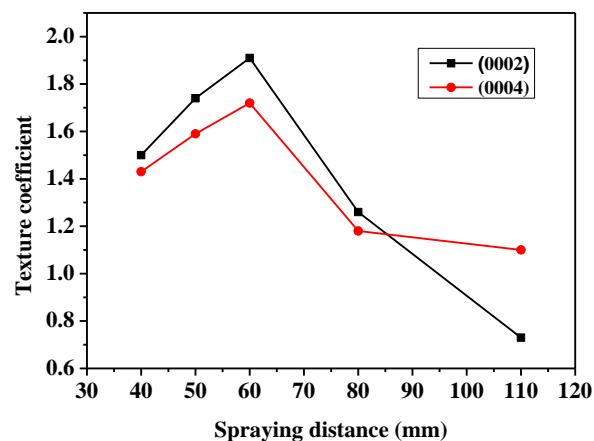
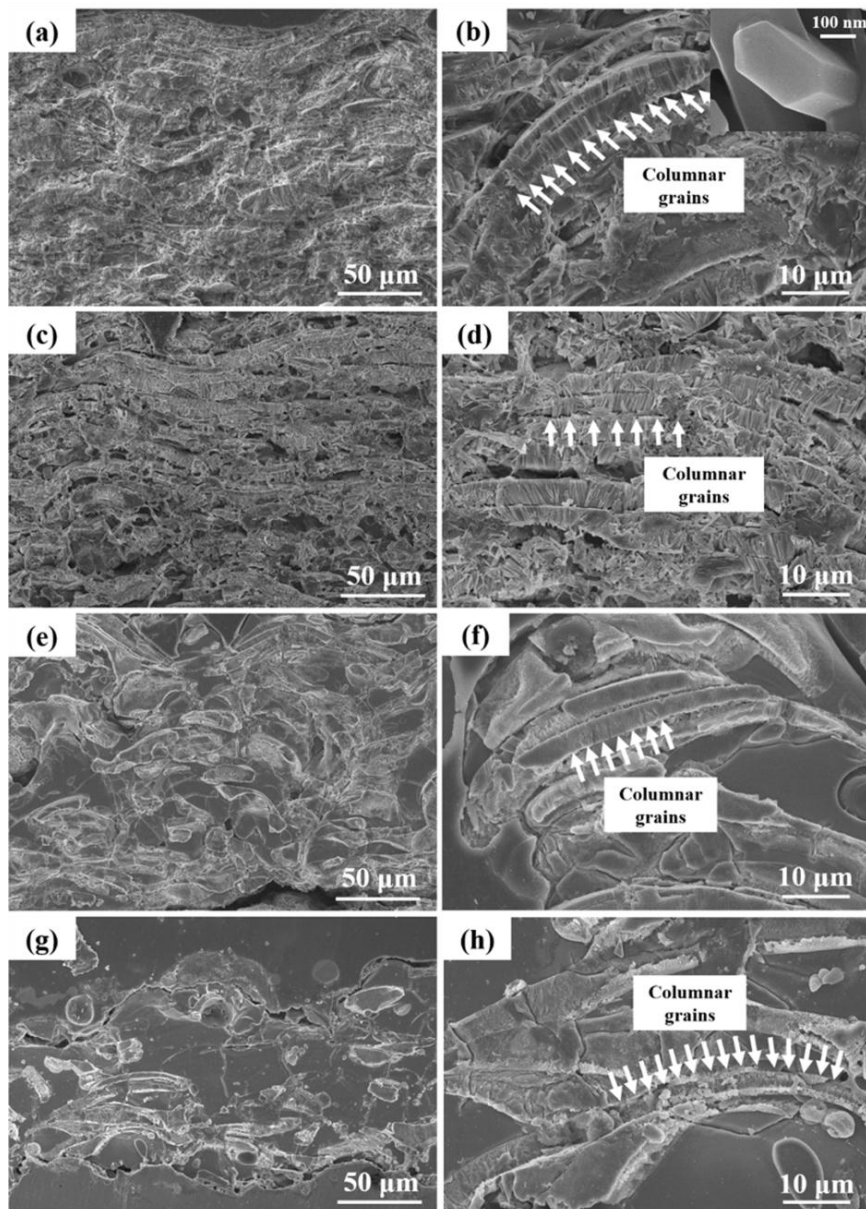


Figure 3. Variations of the texture coefficient for HA coatings deposited at different spraying distances.

Figure 4 shows the SEM micrographs of cross sections of HA coatings at different spraying distances. Samples sprayed at 40 mm showed that partially melted particles exhibited columnar crystals. The columnar grains with hexagons in the coating were in a non-uniform distribution (Figure 4a). In addition, columnar grains extend from the bottom to the top of the HA splat. In some splats, columnar grains are not completely perpendicular to the coating surface (Figure 4b). From the cross-section SEM images of the coating deposited under 60 mm, uniform distribution columnar grains with hexagon sections were observed in the upper part (~100  $\mu\text{m}$ ) (Figure 4c). The cross-section SEM image shows that the columnar grains were parallel to the deposition direction (Figure 4d). However, the morphology of the coatings deposited under 80 and 110 mm changed significantly. These coatings did not have an apparent lamellar structure with columnar grains. In addition, spherical particles were observed deposited at 110 mm. The variation in the columnar grain ratio is in agreement with the evolution of the XRD pattern.



**Figure 4.** Cross-sectional morphology of HA coatings with different spraying distances: (a,b) 40 A, 40 mm; (c,d) 40 A, 60 mm; (e,f) 40 A, 80 mm; (g,h) 40 A, 110 mm.

### 3.2. Microstructure of As-Sprayed Coatings at Different Spraying Currents

Figure 5 shows the XRD patterns of HA coatings sprayed at different spraying currents. Figure 6 shows the calculated values of TC (0002) and TC (0004) for different currents. XRD patterns show that the coating sprayed at 20 A is similar to that of the raw powders, which illustrates that the HA coating deposited at 20 A exhibits a random crystalline orientation. TC (0002) and TC (0004) are below 1. However, the intensity of the peaks (0002) and (0004) of HA coatings at 30 A, 40 A, and 50 A increased. For coating sprayed at 40 A, the decomposition of TTCP,  $\alpha$ -TCP, and ACP decreased. The intensity of peaks (0002) and (0004) increased compared with the coating sprayed at 30 A. Meanwhile, TC (0002) and TC (0004) of the HA coating at 40 A increased. This illustrates that the growth of the (0002) and (0004) preferred orientations is obvious. On the contrary, the intensity of peaks (0002) and (0004) of the HA coating sprayed at 50 A decreased, and TC (0002) and TC (0004) decreased. Meanwhile, the decomposition of TTCP,  $\alpha$ -TCP, and ACP increased. CaO was also observed in this case.

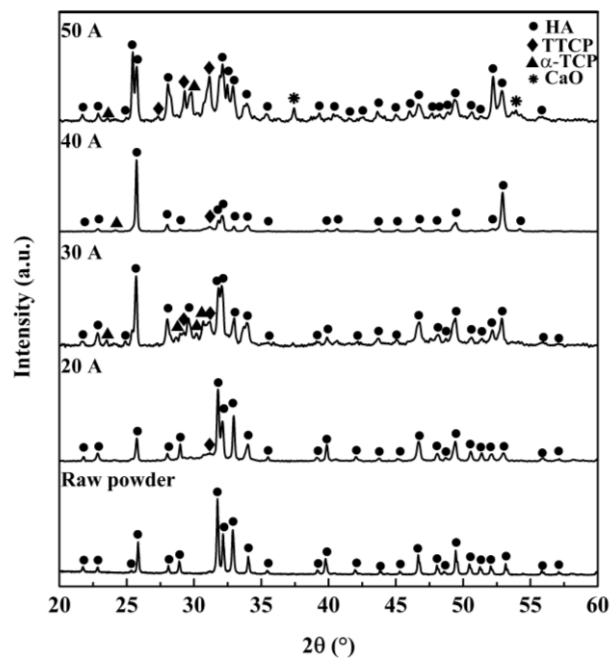


Figure 5. XRD patterns of HA coatings with different spraying currents.

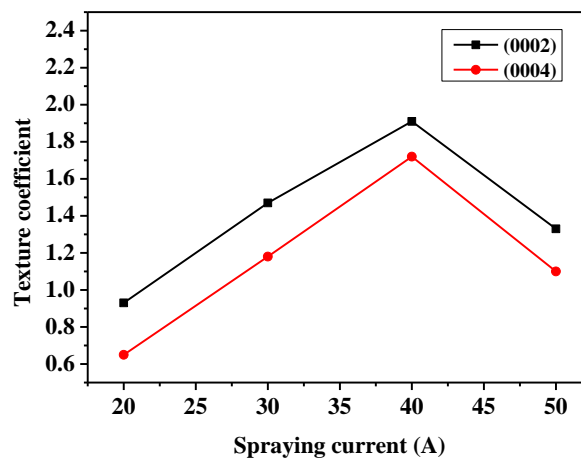
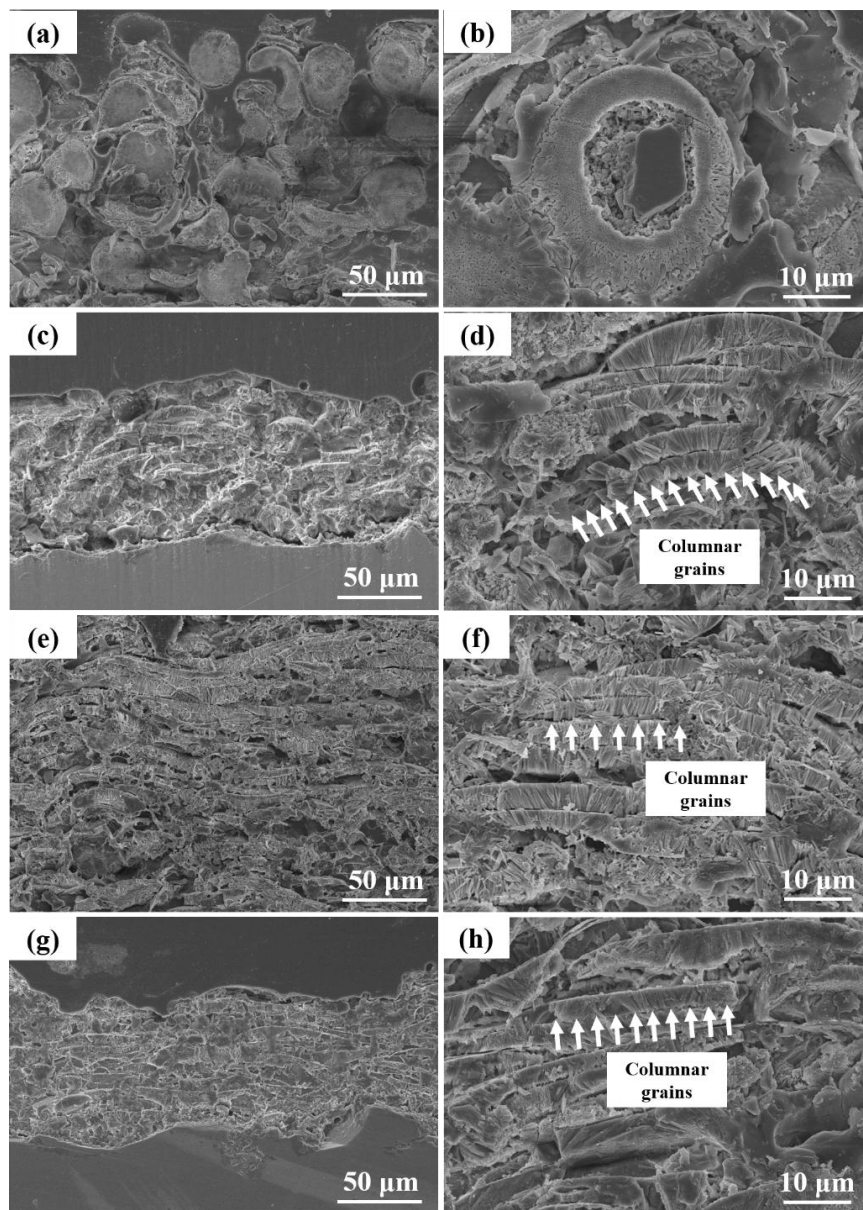


Figure 6. Variations of the texture coefficient for HA coatings deposited at different currents.

SEM micrographics of HA coatings sprayed at different current are shown in Figure 7. The coating sprayed at 20 A shows many unmelted HA particles (Figure 7a). On the other hand, the columnar grains were not observed in this coating (Figure 7b). For the coating sprayed at 30 A, the columnar grains with hexagons were observed in some splats (Figure 7d), and the distribution in the coating is not uniform (Figure 7c). When the spraying current increased to 40 A, the ratio of columnar grains in coatings increased appreciably (Figure 7f). As the spraying current increased, the ratio of columnar grains decreased (Figure 7h). The variation in the columnar grain ratio is in agreement with the evolution of XRD pattern.



**Figure 7.** Cross-sectional morphology of HA coatings with different spraying currents: (a,b) 20 A, 60 mm; (c,b) 30 A, 60 mm; (e,f) 40 A, 60 mm; (g,h) 50 A, 60 mm.

#### 4. Discussion

MPS can be used to obtain HA coatings with strong *c*-axis textures. Through an examination of the microstructure and calculation of the *c*-axis texture coefficient, it was recognized that spraying distance and current have a significant influence on texture.

As we know, the final coating is built up by numberless single splats. In this investigation, the splat types were determined by the particle melting state and substrate condition. In the MPS process, the substrate temperature is significantly higher when the spraying distance is below 60 mm (Figure 8). As a result, the fully melted particles that strike onto the substrate are able to spread out and develop into a disk shape splat. The heat flux of the disk shape splats was perpendicular to the substrate surface, hence promoting the (002) crystal growth along the deposition direction during MPS. During solidification, the columnar grains preferred to grow within disk shape splats. At short spraying distances, the shorter dwell time in the plasma jet is insufficient to melt all the

in-flight particles. The partially melted particles impact the substrate. They are not able to spread out and develop into hemispherical shape splat or disk shape splat. The partially melted particles with lower melting degrees impact the substrate and develop into hemispherical shape splats (Figure 9a). However, partially melted particles with higher melting degrees after impacting the substrate will tend to form disk shape splats (Figure 9b). Columnar grains are not able to form within hemispherical splats. As a result, the columnar grains with hexagons in the coatings deposited at short spraying distances are in a non-uniform distribution.

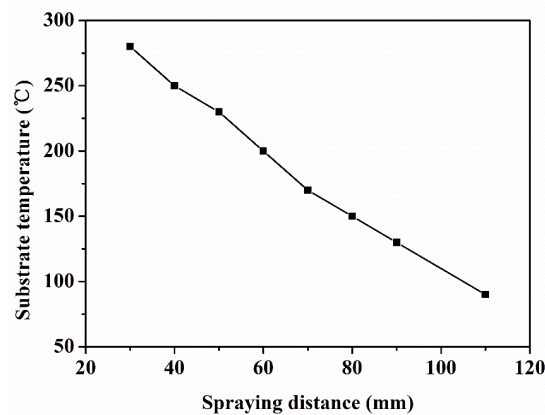


**Figure 8.** Evaluation of substrate temperatures with different spraying distances.

However, columnar grains are not completely perpendicular to the coating surface in some splats. This can be attributed to the fully melted particles striking the hemispherical shape splat, which leads to the reduction of the flattening ratio of fully melted particles. In these splats, the heat flow is not completely perpendicular to the surface of the substrate. Columnar grains grow parallel to heat flow. Consequently, columnar grains are not completely perpendicular to the coating surface in these splats. As spraying distance increased, the velocity of in-flight particles decreased slightly [25], which led to an increase in the dwell time of the in-flight particles in the plasma jet. Therefore, the in-flight particles had been fully melted. Fully melted particles tend to form disk shape splats or splashed shape splats, depending on the substrate temperature. In this study, the plasma jet can act as a heat source and heat the substrate. As the spraying distance decreased, the substrate temperature improved. The fully melted particles struck the heated substrate, which resulted in disk shape splats. As spraying distance increased, substrate temperature decreased because the substrate was further from the plasma jet (Figure 10). In this condition, the lower substrate temperature resulted in splashed shape splats (Figure 9c). The in-flight particles had been fully melted under a spraying distance of 60 mm. In this condition, the splats are dominated by a disk shape splat or limited splashing at its rim. As a result, a dense and uniform coating consisting of columnar grains was formed (Figure 11b), which corresponds to an increased texture coefficient. As spraying further increased, the dwell time of the in-flight particles in the plasma jet increased. On the one hand, increasing the dwell time of in-flight particles caused more HA decomposition and dehydroxylation. On the other hand, as the spraying distance increased, the substrate temperature decreased due to the fact that the substrate was further from the plasma jet. In this case, the splat on the substrate changed from a disk shape to a splashed shape at a rapid cooling rate and thus caused the formation of ACP, but the columnar grains of the HA coatings deposited at 110 mm were not obvious (Figure 11c). In this investigation, when the spraying distance exceeded 80 mm, the in-flight particles moved out of the plasma flame of MPS (Figure 10). The in-flight particles tended to cool down after moving out the plasma flame. Hence, the fine particles surface re-solidified. These particles, which impinge on the substrate, led to the formation of hemispherical shape splats (Figure 9e). As a result, re-solidified particles with a spherical shape were observed in the coating during spraying (Figure 11c).

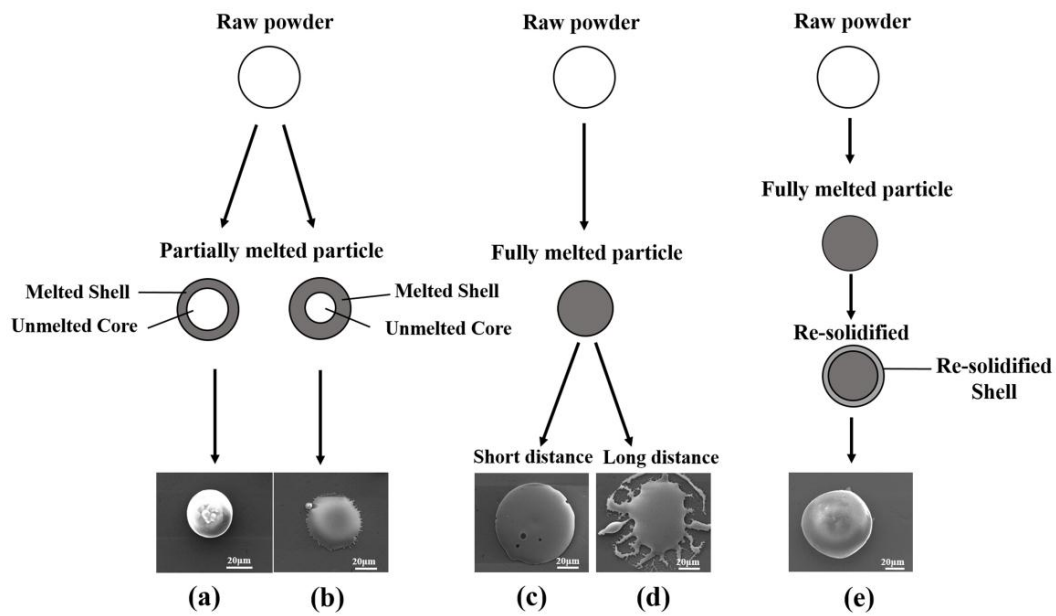


**Figure 9.** Schematic of splat type formation of the single particles during MPS: (a) hemispherical shape splat; (b) oblate spheroidal splat; (c) disk shape splat; (d) splashed shape splat; (e) hemispherical shape splat.

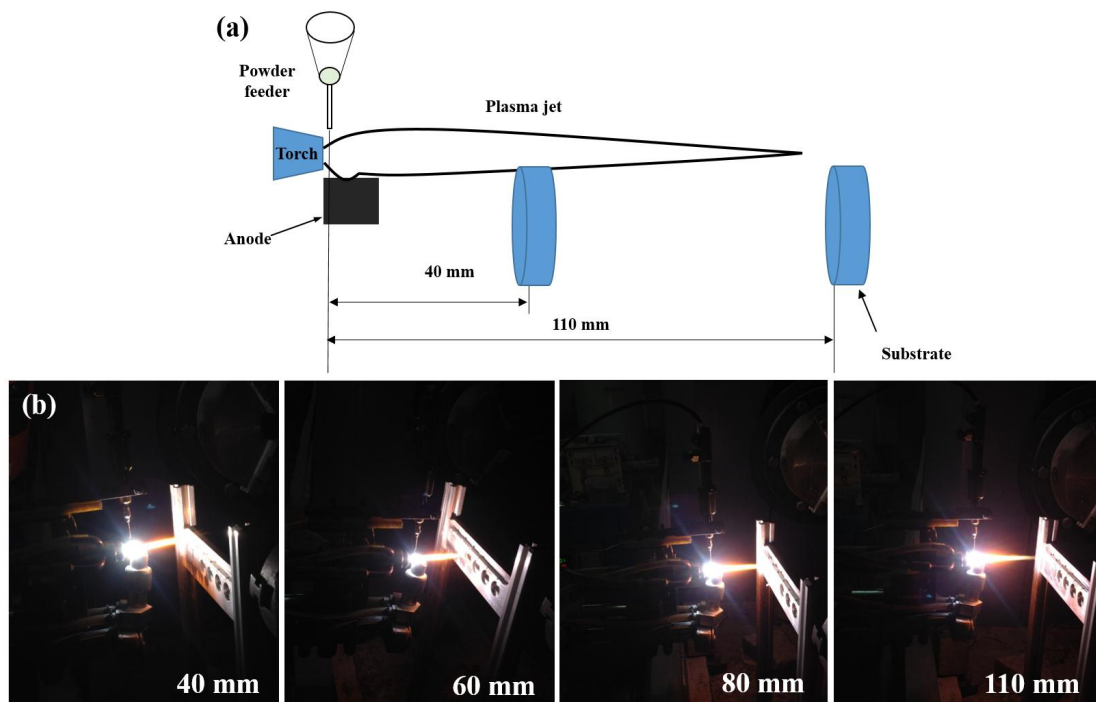


**Figure 10.** (a) Schematic diagram of an MPS torch and (b) the actual experimental conditions during the MPS of HA powder: 40 A, 40 mm; 40 A, 60 mm; 40 A, 80 mm; 40 A, 110 mm.

The coating sprayed at 20 A contains many partially melted particles because the plasma power is insufficient to melt the in-flight particles. The molten shell of the partially melted particle spread out. The unmelted core of the partially melted particles is still present in the splat center (Figure 11a). The size of HA grains located in the unmelted part is much larger than that of those rod-like nanograins in raw powder (Figure 7a,b), which indicates the growth of grains during spraying. Meanwhile,

columnar grains cannot be formed in the unmelted part (Figure 11b). With the increase in spraying current, the temperature of the plasma jet increased. The previous studies showed that the temperature of the plasma jet generally increased as the spraying current increased, and the velocity did not increase significantly [9], which did not significantly decrease the dwell time of in-flight particles in the plasma jet, so the melting degree of the in-flight particles increased as spraying current increased. When the spraying current increased to 40 A, more in-flight particles melted. As a result, more disk shape splats were formed on the substrate. Meanwhile, the proportion of columnar grains was improved, corresponding to the increased *c*-axis orientation intensity of the HA coating in the present experiment. However, when the spraying current exceeded 40 A, the dehydroxylation and decomposition of in-flight particles increased as the plasma temperature increased at a higher spraying power, which enhanced the formation of the impurity phase after the substrate was impacted. Therefore, more HA decomposed. More dehydroxylation and decomposition of HA does not contribute to the formation of columnar grains in the HA coating. In addition, the higher plasma temperature at higher power caused the formation of CaO.

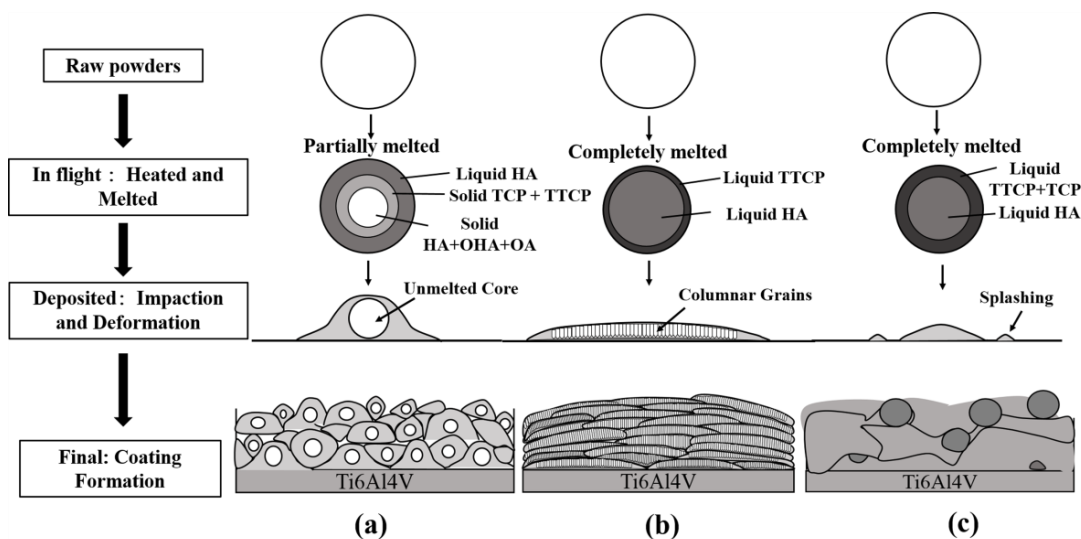


**Figure 11.** Schematic of the formation of three representation HA coatings during MPS: (a) HA coating contains many partially melted particles; (b) HA coating with columnar structure; (c) HA coating with higher amorphous calcium phosphate.

This investigation has shown that columnar grains preferred to grow within disk shape splats. In order to understand the mechanism of this phenomenon, further investigation, such as the cross-section of splat, will be conducted. In addition, further studies will be focused on the investigation of the biological properties of HA coatings with a *c*-axis texture.

## 5. Conclusions

In this paper, we investigated the influence of the process parameters on the texture intensity of MPS-deposited HA coatings. The microstructure of the HA coatings sprayed in different spraying distances and currents was systematically compared and analyzed. From the results, the following can be concluded:

- The process parameters had a significant influence on the phase composition of the coatings. Meanwhile, the texture intensity of the *c*-axis of HA was greatly influenced by spraying distance and spraying current. The strongest *c*-axis texture was found in the coating by 60 mm spraying distance with a spraying current of 40 A. Uniform distribution columnar grains with hexagon sections were observed in the upper part of the coating (~100 μm).

- An increase in the number of fully melted particles was connected to an increase in columnar grain ratio. This can be attributed to the fact that the disk shape splats were formed by fully melted particles and that columnar grains preferred to grow within disk shape splats.
- All the texture intensity variation was ascribed to the growth probability of columnar grains during MPS spraying. The texture intensity in MPS-sprayed HA coatings can be controlled by adjusting the melting state of the in-flight particles and the splat type.

**Acknowledgments:** The authors gratefully appreciate the financial support of the National Natural Science Foundation of China (51471010).

**Author Contributions:** Xiaomei Liu and Dingyong He conceived and designed the experiments; Xiaomei Liu performed the experiments; Xiaomei Liu, Zheng Zhou, Zengjie Wang, and Guohong Wang analyzed the data; Xiaomei Liu and Dingyong He wrote the paper.

**Conflicts of Interest:** The authors declare no conflict of interest.

## References

1. Suchanek, W.; Yoshimura, M. Processing and properties of hydroxyapatite-based biomaterials for use as hard tissue replacement implants. *J. Mater. Res.* **1998**, *13*, 94–117. [[CrossRef](#)]
2. Heimann, R.B. Structure, properties, and biomedical performance of osteoconductive bioceramic coatings. *Surf. Coat. Technol.* **2013**, *233*, 7–28. [[CrossRef](#)]
3. Bhadang, K.A.; Gross, K.A. Influence of fluorapatite on the properties of thermally sprayed hydroxyapatite coatings. *Biomaterials* **2004**, *25*, 4935–4945. [[CrossRef](#)] [[PubMed](#)]
4. Heimann, R.B. Plasma-sprayed hydroxylapatite-based coatings: Chemical, mechanical, microstructural, and biomedical properties. *J. Therm. Spray Technol.* **2016**, *25*, 827–850. [[CrossRef](#)]
5. Vahabzadeh, S.; Roy, M.; Bandyopadhyay, A.; Bose, S. Phase stability and biological property evaluation of plasma sprayed hydroxyapatite coatings for orthopedic and dental applications. *Acta Biomater.* **2005**, *17*, 47–55. [[CrossRef](#)] [[PubMed](#)]
6. Ong, J.L.; Carnes, D.L.; Bessho, K. Evaluation of titanium plasma-sprayed and plasma-sprayed hydroxyapatite implants In Vivo. *Biomaterials* **2004**, *25*, 4601–4606. [[CrossRef](#)] [[PubMed](#)]
7. Chen, Q.; Thouas, G.A. Metallic implant biomaterials. *Mater. Sci. Eng. R Rep.* **2015**, *87*, 1–57. [[CrossRef](#)]
8. Hung, K.Y.; Lai, H.C.; Yang, Y.C.; Feng, H.P. Characterization of hydroxyapatite (HA) sputtering targets by APS methods. *Coatings* **2017**, *7*, 197. [[CrossRef](#)]
9. Zhao, L.; Bobzin, K.; Ernst, F.; Zwick, J.; Lugscheider, E. Study on the influence of plasma spray process and spray parameters on the structure and crystallinity of hydroxyapatite coatings. *Mater. Werkst.* **2006**, *37*, 516–520. [[CrossRef](#)]
10. Ducheyne, P.; Radin, S.; King, L. The effect of calcium phosphate ceramic composition and structure on in vitro behavior. I. Dissolution. *J. Biomed. Mater. Res.* **1993**, *27*, 25–34. [[CrossRef](#)] [[PubMed](#)]
11. Lugscheider, E.; Bobzin, K.; Zhao, L.; Zwick, J. Assessment of the microplasma spraying process for coating application. *Adv. Eng. Mater.* **2006**, *8*, 635–639. [[CrossRef](#)]
12. Surmenev, R.A.; Surmeneva, M.A.; Ivanova, A.A. Significance of calcium phosphate coatings for the enhancement of new bone osteogenesis—A review. *Acta Biomater.* **2014**, *10*, 557–579. [[CrossRef](#)] [[PubMed](#)]
13. Borisov, Y.; Voynarovych, S.G.; Kislitsa, A.N.; Borisova, A.L.; Karpetz, M.V.; Tunik, A.Y. Effect of microplasma spray conditions on structure, phase composition and texture of hydroxyapatite coatings. In Proceedings of the 2006 International Thermal Spray Conference, Seattle, WA, USA, 15–18 May 2006; pp. 29–34.
14. Wang, Y.M.; Fan, T.T.; Zhou, Z.; He, D.Y. Hydroxyapatite coating with strong (002) crystallographic texture deposited by micro-plasma spraying. *Mater. Lett.* **2016**, *185*, 484–487. [[CrossRef](#)]
15. Dey, A.; Mukhopadhyay, A.K.; Gangadharan, S.; Sinha, M.K.; Basu, D. Characterization of microplasma sprayed hydroxyapatite coating. *J. Therm. Spray Technol.* **2009**, *18*, 578–592. [[CrossRef](#)]
16. Roy, M.; Bandyopadhyay, A.; Bose, S. Induction plasma sprayed nano hydroxyapatite coatings on titanium for orthopaedic and dental implants. *Surf. Coat. Technol.* **2011**, *205*, 2785–2792. [[CrossRef](#)] [[PubMed](#)]
17. Almora-Barrios, N.; Austen, K.F.; de Leeuw, N.H. Density functional theory study of the binding of glycine, proline, and hydroxyproline to the hydroxyapatite (0001) and (0110) surfaces. *Langmuir* **2009**, *25*, 5018–5025. [[CrossRef](#)] [[PubMed](#)]

18. Dong, X.L.; Zhou, H.L.; Wu, T.; Wang, Q. Behavior regulation of adsorbed proteins via hydroxyapatite surface texture control. *J. Phys. Chem. C* **2008**, *112*, 4751–4759. [[CrossRef](#)] [[PubMed](#)]
19. Wang, Y.M.; Liu, X.M.; Fan, T.T.; Tan, Z.; Zhou, Z.; He, D.Y. In vitro evaluation of hydroxyapatite coatings with (002) crystallographic texture deposited by micro-plasma spraying. *Mater. Sci. Eng. C* **2017**, *75*, 596–601. [[CrossRef](#)] [[PubMed](#)]
20. Kim, H.; Camata, R.P.; Chowdhury, S.; Vohra, Y.K. In vitro dissolution and mechanical behavior of the *c*-axis preferentially oriented hydroxyapatite thin films fabricated by pulsed laser deposition. *Acta Biomater.* **2010**, *6*, 3234–3241. [[CrossRef](#)] [[PubMed](#)]
21. Dinu, M.; Ivanova, A.A.; Surmeneva, M.A.; Braic, M.; Tyurin, A.I.; Braic, V.; Vladescu, A. Tribological behaviour of RF-magnetron sputter deposited hydroxyapatite coatings in physiological solution. *Ceram. Int.* **2017**, *43*, 6858–6867. [[CrossRef](#)]
22. Ivanova, A.A.; Surmeneva, M.A.; Surmenev, R.A.; Depla, D. Influence of deposition conditions on the composition, texture and microstructure of RF-magnetron sputter-deposited hydroxyapatite thin films. *Thin Solid Films* **2015**, *591*, 368–374. [[CrossRef](#)]
23. Ivanova, A.A.; Surmeneva, M.A.; Surmenev, R.A.; Depla, D. Structural evolution and growth mechanisms of RF-magnetron sputter-deposited hydroxyapatite thin films on the basis of unified principles. *Appl. Surf. Sci.* **2017**, *425*, 497–506. [[CrossRef](#)]
24. Fanni, L.; Aebersold, B.A.; Alexander, D.T.L.; Ding, L.; Morales Masis, M.; Nicolay, S.; Ballif, C. *c*-texture versus *a*-texture low pressure metalorganic chemical vapor deposition ZnO films: Lower resistivity despite smaller grain size. *Thin Solid Films* **2014**, *565*, 1–6. [[CrossRef](#)]
25. Liu, X.M.; He, D.Y.; Wang, Y.M.; Zhou, Z.; Wang, G.H.; Tan, Z.; Wang, Z.J. The influence of spray parameters on the characteristics of hydroxyapatite in-flight particles, splats and coatings by micro-plasma spraying. *J. Therm. Spray Technol.* **2018**. [[CrossRef](#)]



© 2018 by the authors. Licensee MDPI, Basel, Switzerland. This article is an open access article distributed under the terms and conditions of the Creative Commons Attribution (CC BY) license (<http://creativecommons.org/licenses/by/4.0/>).